Mechanism-Based Inactivation of CYP2B1 and Its F-Helix Mutant by Two *tert*-Butyl Acetylenic Compounds: Covalent Modification of Prosthetic Heme Versus Apoprotein

Hsia-lien Lin, Haoming Zhang, Kathleen R. Noon, and Paul F. Hollenberg

Department of Pharmacology, University of Michigan, Ann Arbor, Michigan

ABSTRACT

The mechanism-based inactivation of cytochrome CYP2B1 [wild type (WT)] and its Thr205 to Ala mutant (T205A) by *tert*-butylphenylacetylene (BPA) and *tert*-butyl 1-methyl-2-propynyl ether (BMP) in the reconstituted system was investigated. The inactivation of WT by BPA exhibited a k_{inact}/K_I value of 1343 $min^{-1}mM^{-1}$ and a partition ratio of 1. The inactivation of WT by BMP exhibited a k_{inact}/K_I value of 33 $min^{-1}mM^{-1}$ and a partition ratio of 10. Liquid chromatography/tandem mass spectrometry analysis (LC/MS/MS) of the WT revealed 1) inactivation by BPA resulted in the formation of a protein adduct with a mass increase equivalent to the mass of BPA plus one oxygen atom, and 2) inactivation by BMP resulted in the formation of multiple heme adducts that all exhibited a mass increase equivalent to BMP plus one oxygen atom. LC/MS/MS analysis indi-cated the formation of glutathione (GSH) conjugates by the reaction of GSH with the ethynyl moiety of BMP or BPA with the oxygen being added to the internal or terminal carbon. For the inactivation of T205A by BPA and BMP, the k_{inact}/K_I values were suppressed by 100- and 4-fold, respectively, and the partition ratios were increased 9- and 3.5-fold, respectively. Only one major heme adduct was detected following the inactivation of the T205A by BMP. These results show that the Thr205 in the F-helix plays an important role in the efficiency of the mechanism-based inactivation of CYP2B1 by BPA and BMP. Homology modeling and substrate docking studies were presented to facilitate the interpretation of the experimental results.

The cytochrome P450 (P450) 2B enzymes catalyze the metabolism of a wide variety of endogenous and exogenous substrates, including clinically used drugs, chemical carcinogens, steroids, and environmental pollutants. In the past 5 years the crystal structures of ligand-free, 4-(4-chlorophenyl) imidazole-bound, and bifonazole-bound CYP2B4 have revealed that conformational changes in several regions of CYP2B4 can dramatically reshape the active site of the enzyme to fit the size and shape of the bound ligand (Scott et al., 2003, 2004; Zhao et al., 2006). With ligand-bound, the F-G region of CYP2B4 further stabilizes the closed conformation by capping the active site on top of B′-helix or forms a crystallographic dimer in which the F-G region of one molecule inserts into the widely open active site cleft of the symmetrically related molecule and vice versa. In the CYPBM3-substrate complex, the F-G region exhibits a rocking motion with the I-helix as a fulcrum in the substrate-docking region to position the substrate for catalysis (Haines et al., 2001). Thus, it appears that the F-helix residues may be prime targets to study to gain information about the relationship between the structure and function of these proteins. The contributions of several amino acids in the F-helix to substrate specificity and the regio- and stereoselectivity of product formation have been shown for members of the CYP2 family (Lindberg and Negishi, 1989; Domanski and Halpert, 2001; Kirton et al., 2002; Guengerich et al., 2003; Lin et al., 2003, 2004; Spatzenegger et al., 2003). The combination of approaches involving mechanism-based inactivators and site-directed mutagenesis has played an important role in studies on the structure-function relationships of P450s, in particular P450 2B (Zhao and Halpert, 2007). Although the efficiency of inactivation by 2-ethynylnaphthalene and 17α-ethynylestradiol is not significantly altered in the Thr205 to Ala (T205A) mutant of CYP2B1, the regioselectivity for the formation of metabolites of testosterone, androstenedione,

ABBREVIATIONS: P450, cytochrome P450; WT, wild type; BPA, 4-*tert*-butylphenylacetylene; BMP, *tert*-butyl 1-methyl-2-propynyl ether; GSH, glutathione; DLPC, dilauroyl-L-α-phosphatidylcholine; EFC, 7-ethoxy-4-(trifluoromethyl)coumarin; HPLC, high-pressure liquid chromatography; TFA, trifluoroacetic acid; ESI, electrospray ionization; LC/MS/MS, liquid chromatography/tandem mass spectrometry; SRS, substrate recognition site.

tert-butyl 1-methyl-2-propynyl ether (BMP)
MW = 126 g/mol

4-tert-butylphenylacetylene (BPA)
MW = 158 g/mol
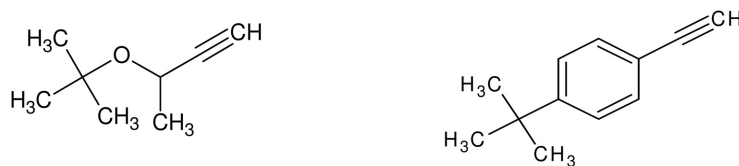
Fig. 1. Structures of the two *tert*-butyl acetylenic compounds: BMP and BPA.

and 17α-ethynylestradiol by the T205A mutant is different from that of wild type (WT) (Lin et al., 2003, 2004), suggesting that the functional role of a given residue may be substrate-dependent. Therefore, we investigated the inactivation of WT CYP2B1 and its T205A mutant by 4-*tert*-butylphenylacetylene (BPA) and *tert*-butyl 1-methyl-2-propynyl ether (BMP). These two *tert*-butyl acetylenic compounds are structurally related, as shown in Fig. 1.

BMP has been shown to cause mechanism-based inactivation of CYP2B1 as a result of loss of prosthetic heme with the concomitant formation of heme adducts (von Weymarn et al., 2004). Previous studies on P450s purified from phenobarbital-induced rat liver have shown that catalytic activity is lost in an NADPH- and time-dependent manner when they are incubated with several substituted phenylacetylenes and that the mechanism of inactivation involved heme alkylation (Komives and Ortiz de Montellano, 1987). However, inactivation by a phenylacetylene such as BPA having a *tert*-butyl group has not yet been characterized. Therefore, we have characterized the mechanism-based inactivation of the WT CYP2B1 and the T205A mutant by these two *tert*-butyl acetylenic compounds. By comparing the WT and mutant P450s, a possible role for the Thr residue at position 205 in the metabolism of these two acetylenes has been identified.

The covalent binding of ethynyl compounds to the prosthetic heme moiety or to the apoprotein has been shown previously (Ortiz de Montellano and Komives, 1985; CaJacob et al., 1988; Chan et al., 1993). Whether the inactivation results from alkylation of the prosthetic heme or modification of the apoprotein appears to be determined by the site of addition of the oxygen at either the internal or terminal carbon of the carbon-carbon triple bond, respectively. Covalent binding of the reactive intermediate to both the heme moiety and the apoprotein has been shown for the inactivation of CYP3A4 and CYP3A5 by 17α-ethynylestradiol (Lin et al., 2002; Lin and Hollenberg, 2007). However, the factors determining which carbon of the triple bond the oxygen is added to are not clear. It is interesting to note that these two structurally related *tert*-butyl acetylenic compounds inactivate CYP2B1 by two distinct mechanisms and that the efficiency of inactivation by BPA is 70-fold greater than that by BMP. Moreover, when Ala was substituted for Thr at position 205, the decrease of the efficiency of inactivation by BPA and BMP was 100- and 4-fold, respectively. In short, Thr205 is much more critical for the inactivation of CYP2B1 by BPA than for the inactivation by BMP. Homology modeling and docking studies of these two acetylenes in the CYP2B1 active site support the experimental results.

Materials and Methods

Chemicals. Catalase, NADPH, glutathione (GSH), dilauroyl-L-α-phosphatidylcholine (DLPC), BMP, and BPA were purchased from Sigma-Aldrich (St. Louis, MO). 7-Ethoxy-4-(trifluoromethyl)coumarin (EFC) was from Invitrogen (Carlsbad, CA). All the other chemicals and solvents were of the highest purity available from commercial sources.

Purification of Enzymes. The site-specific mutation of Thr205 to Ala in CYP2B1 and the purification of the P450s were performed as described previously (Lin et al., 2003). Reductase was expressed in *Escherichia coli* and purified according to previous published procedures (Lin et al., 2003).

Enzyme Assay and Inactivation of P450s. To assess catalytic activity, the purified P450s and reductase were reconstituted with DLPC at 22°C for 30 min as described previously (Lin et al., 2004). The primary reaction mixture contained 500 pmol of P450, 500 pmol of reductase, 50 μg of DLPC, 2 mM GSH, 100 units of catalase, and BMP (3–50 μM) or BPA (0.3–25 μM) in 500 μl of 100 mM potassium phosphate buffer, pH 7.7. After incubation of the primary reaction in the presence of 1 mM NADPH at 22°C with BMP or BPA for the time indicated (0.5–6 min), a 10-μl aliquot was removed and added to 1 ml of a secondary reaction mixture containing 100 μM EFC and 200 μM NADPH. Measurements of catalytic activity and calculations of kinetic values for mechanism-based inactivation were performed as described previously (Kent et al., 2002; Lin et al., 2004).

Determination of the Partition Ratios. BMP at concentrations ranging from 2.5 to 300 μM or BPA at concentrations ranging from 0.6 to 100 μM was added to the primary reaction mixture containing 1 μM P450. The reactions were initiated by the addition of 1 mM NADPH and incubated at 22°C for 30 min to allow the inactivation to go to completion (Silverman, 1996). Aliquots were removed and assayed for residual EFC activity as described above.

High-Pressure Liquid Chromatography Analysis of the Heme Adducts. A high-pressure liquid chromatography (HPLC) system with a Waters (Milford, MA) 600E system controller was used to investigate the loss of native heme and the formation of heme adducts. Aliquots containing 100 pmol of control (−NADPH) and inactivated (+NADPH) P450, incubated with 10 μM BPA or 25 μM BMP for 5 min as described above for the inactivation, were then analyzed using a C4 reverse-phase column (5 μm, 4.6 × 250 mm, 300 Å; Phenomenex, Torrance, CA). The solvent system consisted of solvent A [0.1% trifluoroacetic acid (TFA) in water] and solvent B (0.05% TFA in acetonitrile). The column was eluted with a linear gradient from 30% to 80% B over 30 min at a flow rate of 1 ml/min, and the column eluant was monitored at 405 nm.

Electrospray Ionization/Liquid Chromatography/Mass Spectrometry Analysis of the Apoprotein. The control (−NADPH) and samples inactivated (+NADPH) by incubation with 10 μM BPA for 2 min or 50 μM BMP for 10 min were prepared. Aliquots (originally containing 50 pmol of P450) were analyzed on a C3 reverse-phase column (Zorbax 300SB-C3, 3.5 μm, 3.0 × 150 mm; Agilent Technologies, Wilmington, DE) equilibrated with 40% acetonitrile and 0.1% TFA. After 5 min, the column effluent was directed into the mass

WT/BPA

T205A/BPA
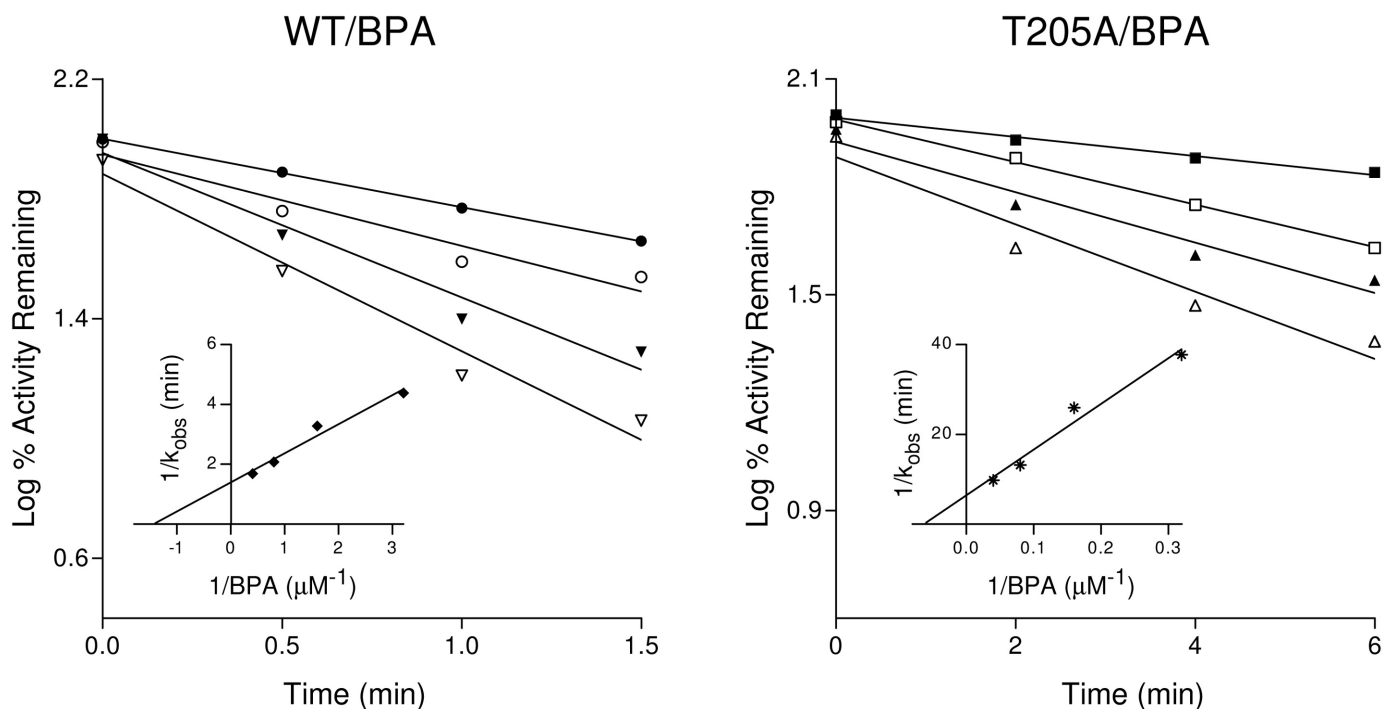
Fig. 2. Time- and concentration-dependent loss of EFC de-ethylation activity for the WT and T205A mutant of CYP2B1 during inactivation by BPA. The reconstituted system containing the WT was incubated with 0.31 μM (●), 0.62 μM (○), 1.25 μM (▼), and 2.5 μM (▽) BPA, and the T205A mutant was incubated with 3.1 μM (■), 6.2 μM (□), 12.5 μM (▲), and 25 μM (△) BPA. Aliquots were removed at the times indicated and assayed for residual EFC de-ethylation activity as described under *Materials and Methods*. The insets show the double reciprocal plots of the kinetic constants obtained from the initial plots. The K_I and k_{inact} values were determined from the double reciprocal plots. The data represent the average of three separate experiments done in duplicate that did not differ by >10%.

TABLE 1

Kinetic values for inactivation and partition ratios for the WT and T205A mutant P450s inactivated by BPA and BMP[a]

Inactivator	P450	K_I	k_{inact}	k_{inact}/K_I	Partition Ratio[b]
		μM	min⁻¹	min⁻¹mM⁻¹	
BPA	WT	0.7	1.64	2343	1
	T205A	16	0.36	23	9
BMP	WT	17	0.56	33	10
	T205A	16	0.14	9	35

[a] The kinetic values were determined as described under *Materials and Methods* and in Fig. 2.
[b] The partition ratios were determined as described in Fig. 3.

analyzer of an LCQ mass spectrometer (Thermo Fisher Scientific, San Jose, CA) as described previously (Kent et al., 2006). The acetonitrile concentration was increased linearly to 90% over the next 25 min to separate the components of the reconstitution mixture, and the mass spectra were recorded. The *m/z* spectra corresponding to the protein envelopes for the P450s were deconvoluted to give the masses associated with each protein envelope using the Bioworks software package (Thermo Fisher Scientific). The electrospray ionization (ESI) source conditions were sheath gas set at 90 arbitrary units; the auxiliary gas was set at 30 arbitrary units; the spray voltage was 4.2 kV; and the capillary temperature was 230°C.

Liquid Chromatography/Tandem Mass Spectrometry Analysis of GSH Conjugates. The control and inactivated samples for WT CYP2B1 and the T205A mutant were prepared as described above. After the 20-min reaction, samples containing 1 nmol each of P450 were acidified with 60 μl of 10% TFA and then applied to a 1-ml AccuBond ODS-C18 solid-phase extraction cartridge (Agilent Technologies). The cartridges were previously washed with 2 ml of methanol followed by 2 ml of water. After the samples were loaded, the cartridges were washed with 2 ml of water and then eluted with 2 ml of methanol followed by 0.3 ml of acetonitrile. The eluted samples were dried under N₂ gas and resuspended in 80 μl of a 1:1 mixture

of solvent A (0.1% acetic acid in H₂O) and solvent B (0.1% acetic acid in acetonitrile). The samples were analyzed on a C18 reverse-phase column (Luna, 3 μm, 4.6 × 100 mm; Phenomenex) using a gradient of 20 to 30% B over 5 min followed by a gradient to 40% B over 15 min and then increasing linearly to 90% B over 15 min at a flow rate of 0.3 ml/min. The column effluent was directed into the ESI source of an LCQ mass spectrometer (Thermo Fisher Scientific). The ESI conditions were sheath gas flow rate, 90 arbitrary units; auxiliary gas, 30 arbitrary units; spray voltage, 4.5 kV; capillary temperature, 170°C; capillary voltage, 30 V; and tube lens offset, 25 V. Data were acquired in positive ion mode using Xcalibur software (Thermo Fisher Scientific) with one full scan followed by two data-dependent scans of the most intense and the second most intense ions.

Liquid Chromatography/Tandem Mass Spectrometry Analysis of Heme Adducts. The purified P450s and reductase were reconstituted as described previously. Samples containing 50 pmol of CYP2B1, 50 pmol of reductase, 2.5 μg of DLPC, 2 mM GSH, 5 units of catalase, and 1 mM NADPH were incubated with 50 μM BMP at 22°C for 20 min and then subjected to liquid chromatography/tandem mass spectrometry (LC/MS/MS) analysis. Experiments were carried out using a Thermo Fisher Scientific LTQ linear ion trap mass spectrometer equipped with the Thermo Fisher Scientific Surveyor HPLC system. The ESI source was tuned with the heme moiety from horse heart myoglobin to optimize the conditions. The source parameters were 4 kV for the spray voltage, 300°C for the capillary temperature, 47 V for the capillary voltage, 100 V for the tube lens, 30 for the sheath gas, and 5 for the auxiliary gas. The ion trap was operated in the positive ion mode. An aliquot (25 pmol) of the primary reaction mixtures inactivated by incubation with BMP was injected onto a reverse-phase HPLC column (XTerra MS C18, 2.1 × 150 mm; Waters) equilibrated with 65% solvent A (0.05% TFA/0.05% formic acid) and 35% solvent B (0.05% TFA/0.05% formic acid in acetonitrile) at a flow rate of 0.3 ml/min. The column was held at 35% solvent B for 5 min, increased linearly to 80% solvent B over 40 min, then ramped to 95% solvent B over 10 min. The effluent from
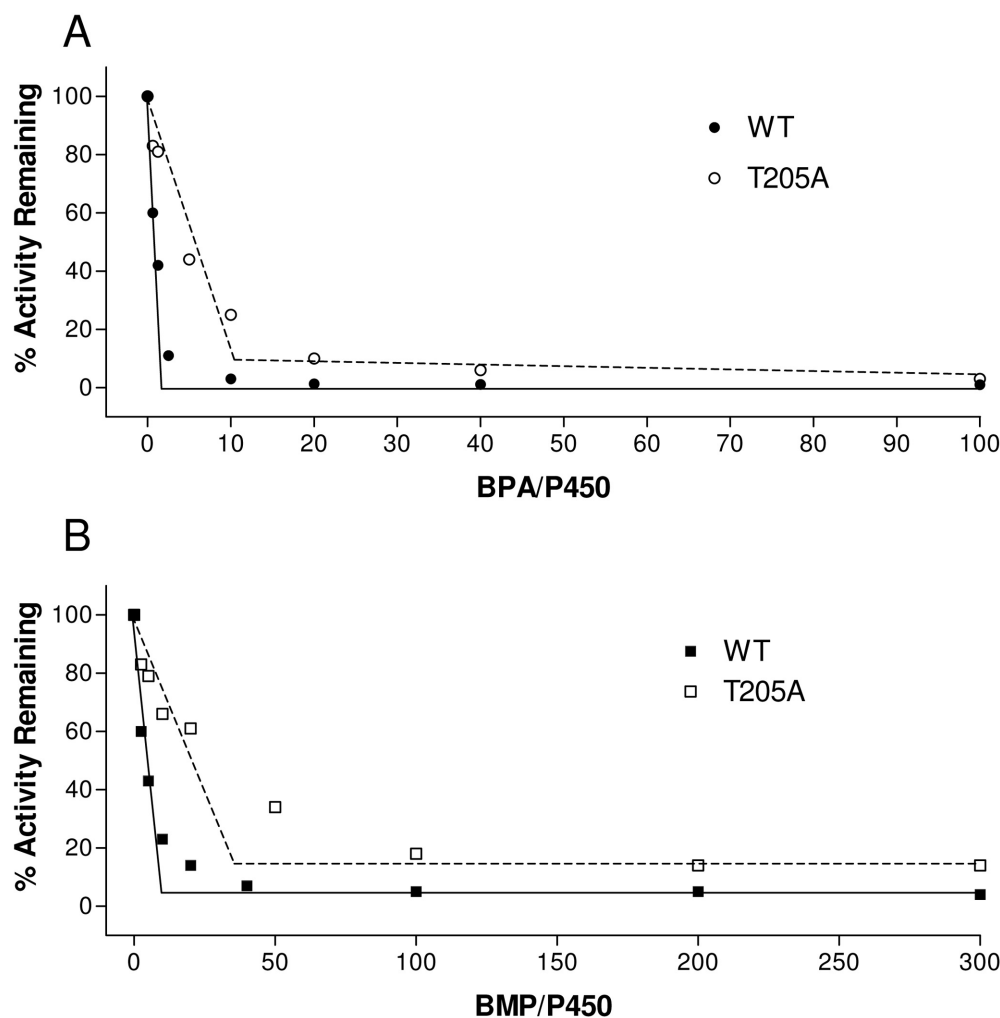
Fig. 3. Determination of partition ratios for the inactivation of the WT and T205A mutant P450s by BPA (A) and BMP (B). The percentage of catalytic activity remaining was determined as a function of the molar ratio of BPA or BMP to the P450s as described under *Materials and Methods*. The partition ratios were estimated from the intercept of the linear regression line from the lower ratios of each inactivator to the P450s and the straight line obtained from higher ratios of each inactivator to the P450s.

the HPLC was directed into the ESI probe of the ion trap. Full-scan data were collected from *m/z* 300 to 2000, and MS/MS spectra were acquired in a data-dependent mode on the six most abundant ions in the survey scan. The normalized collision energy was set to 35%.

Docking of Substrates in the CYP2B1 Active Site. BPA and BMP were docked into the active site of CYP2B1 using the energy-based docking software of AutoDock (version 4.0) (Morris et al., 1996). A homology model of CYP2B1 was constructed based on a template of the CYP2B4 crystal structure (Protein Data Bank code 1SUO) (Scott et al., 2004). The coordinates for BPA and BMP were built using ChemBioOffice 2008 (CambridgeSoft Corporation, Cambridge, MA), and their lowest energy conformations were obtained using the AM1 method. The flexible BPA and BMP ligands were docked to the rigid CYP2B1 using the Lamarckian genetic algorithm approach of AutoDock 4 with the following parameters: mutation rate = 0.02; crossover = 0.80; maximal number of generations = 2.7×10^7; local search frequency = 0.06.

Results

Inactivation of P450s. The inactivation of the EFC deethylation activity of the WT and T205A mutant P450s by BPA and BMP was measured using various concentrations of the acetylenic substrates and various time points at each concentration. The inactivation of WT CY2B1 and T205A mutant by BPA was time- and concentration-dependent (Fig. 2). Linear regression analysis of the time course data was used to estimate the initial rate constants (k_{obs}) for the inac-

tivation of the P450s by BPA. From the double reciprocal plots (inset) of the values for k_{obs} and the concentration of BPA, the kinetic values for the K_I and k_{inact} were calculated essentially as described previously, and the efficiency of inactivation is expressed as k_{inact}/K_I (Roberts et al., 1998; Kent et al., 2002; Lin et al., 2004). Similar results were observed for the inactivation of the WT and mutant enzymes by BMP (data not shown). All of the kinetic values are summarized in Table 1. BPA is ~70-fold (2343 versus 33) more efficient for the inactivation of the WT enzyme than BMP. For the Thr205 to Ala mutant, the k_{inact} was altered 4-fold, but not the K_I for the inactivation by BMP, whereas both the K_I and k_{inact} were markedly altered for inactivation by BPA. Thus, the mutation of Thr to Ala resulted in an ~100-fold (2343 versus 23) decrease in the efficiency of inactivation by BPA and only ~4-fold (33 versus 9) by BMP.

Partition Ratios for the Inactivations. The P450s were incubated with various concentrations of BPA or BMP for 30 min for the inactivation to reach completion. The percentage of activity remaining was plotted as a function of the molecular ratio of inactivator to P450 (Fig. 3.) The turnover number (partition ratio + 1) was estimated from the intercept of the linear regression line obtained from the lower ratios of inactivator to P450 with the straight line derived from higher ratios of inactivator to P450 (Silverman, 1996). The partition ratios for the inactivation of both P450s by BPA and BMP
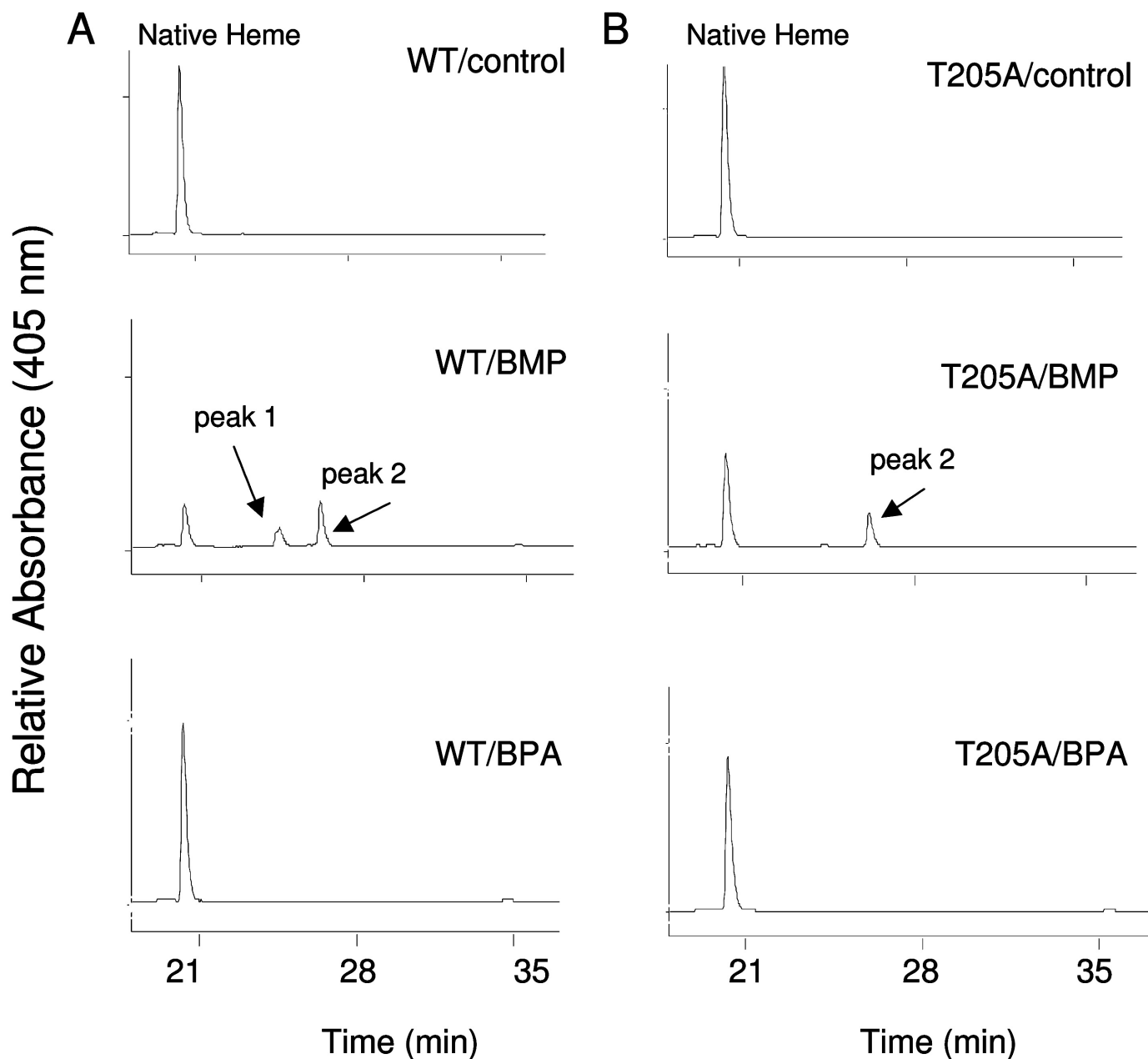
Fig. 4. HPLC elution profiles for the reconstituted system after incubating the WT (A) or T205A mutant (B) 2B1 with BPA or BMP as described under *Materials and Methods*. WT/control and T205A/control are the reaction mixtures incubated without NADPH. WT/BMP, WT/BPA, T205A/BMP, and T205A/BPA are the reaction mixtures incubated with inactivator and NADPH. Native heme, peak 1, and peak 2 eluted at 20, 24, and 26 min, respectively.

were estimated, and they are summarized in Table 1. The lower partition ratio for the WT compared with the T205A mutant indicates that fewer molecules of BPA or BMP for WT were metabolized for every one molecule of P450 that became inactivated. In the WT, the lower partition ratio for BPA compared with BMP indicates that BPA is more efficient as an inactivator.

Changes in the Prosthetic Heme Moiety. The reaction mixtures containing the WT or T205A mutant P450s were incubated with 10 μM BPA or 50 μM BMP for 5 min in the absence (WT/control and T205A/control) or presence of NADPH (WT/BPA, WT/BMP, T205A/BPA, and T205A/BMP). As shown in Fig. 4, the samples were analyzed by HPLC, and the elution profiles were monitored at 405 nm for native

heme remaining (eluting at 20 min) and the formation of heme adduct peak 1 (eluting at 24 min) and heme adduct peak 2 (eluting at 26 min). For WT/BMP, the native heme remaining and EFC catalytic activity remaining is ~20 and ~24% of WT/control, respectively. For T205A/BMP, the native heme remaining and EFC catalytic activity remaining is ~43 and ~42% of T205A/control, respectively. In contrast, there was no significant loss of native heme for WT/BPA and T205A/BPA when EFC catalytic activity remaining was only ~5 and ~24% with respect to their controls, respectively. These results indicate that heme destruction is the major contributor to the inactivation of both WT and T205A by BMP but not by BPA.

For WT/BMP, the absorbance of native heme, peak 1, and
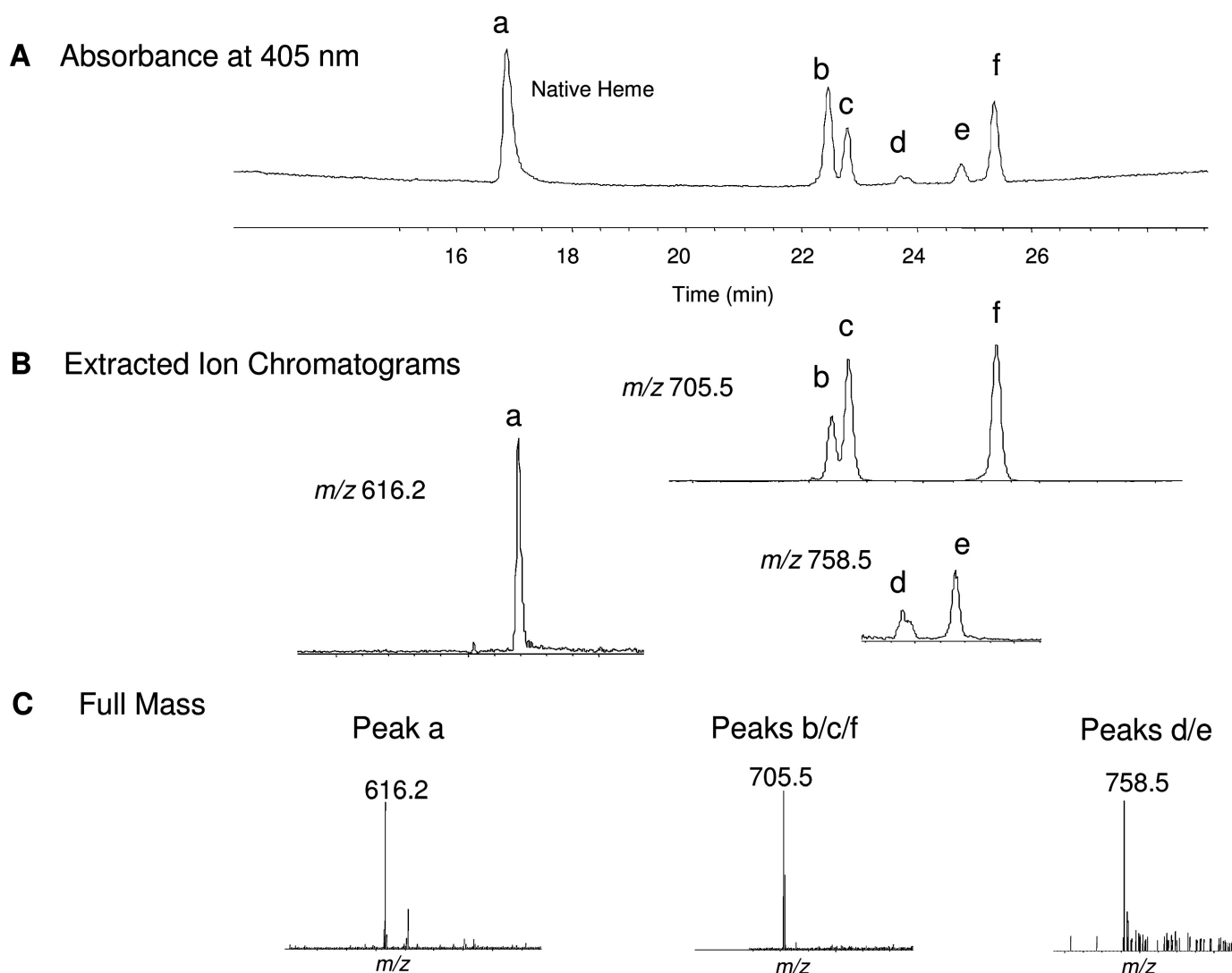
Fig. 5. Analysis of CYP2B1 heme adducts after incubating the reaction mixture with BMP and NADPH. After inactivation of WT by BMP, as described under *Materials and Methods*, the reaction mixture was injected directly onto a reverse-phase HPLC column, and the effluent was analyzed using a photodiode-array detector and a Thermo Fisher Scientific LTQ linear ion trap mass spectrometer as described under *Materials and Methods*. A, HPLC elution profile for peaks a, b, c, d, e, and f monitored at 405 nm. B, the extracted ion chromatograms for each of the peaks observed in the HPLC elution profile. C, the full mass spectra for peak a having *m/z* 616.2, peaks b, c, and f having *m/z* values 705.5, and peaks d and e having *m/z* 758.5.

peak 2 is ~20, ~10, and ~22% of the WT/control, respectively. For T205A/BMP, the absorbance of native heme, peak 1, and peak 2 is ~43, ~1, and ~14% of the T205A/control. These results indicate that substitution of the Thr at the position 205 with Ala attenuated the destruction of native heme and selectively abolished the formation of peak 1.

LC/MS/MS Analysis of the Heme Adducts Formed with BMP. It appears that the heme adduct peak 1 shown in Fig. 4A was not a single homogeneous peak. Therefore, we used LC/MS/MS analysis with a high-resolution HPLC column to further characterize the masses of the heme adducts. Figure 5A shows that four major (a, b, c, and f) and two minor (d and e) heme-derived peaks were now detected in the HPLC profile when monitoring the absorbance at 405 nm after inactivation of CYP2B1 by BMP. The maximal photodiode-array absorption spectra of peak a, peak b/c, peak d/e, and peak f were at 398, 411, 402, and 405 nm, respectively (data not shown). Figure 5B shows the following; 1) the extracted ion chromatogram for peak a with the MH$^+$ ion at *m/z* 616.2

is that of the native heme; 2) the extracted ion chromatograms for peaks b, c, and f with MH$^+$ ions at *m/z* 705.5 are the equivalent of alkylation of the Fe-free prosthetic heme by BMP plus one oxygen atom; and 3) the extracted ion chromatograms for peaks d and e with MH$^+$ ions at *m/z* 758.5 are the equivalent of alkylation of the Fe-containing prosthetic heme by BMP plus one oxygen atom. The full mass spectra for the native heme, Fe-free heme adducts with precursor ions at *m/z* 705.5 and the Fe-containing heme adducts with precursor ions at *m/z* 758.5 are displayed in Fig. 5C. The MS/MS spectra of the major heme adduct with ions at *m/z* 705.5 have previously been reported (von Weymarn et al., 2004). The heme adducts with MH$^+$ ions at *m/z* 758.5 were not abundant, and their analysis was hampered by the presence of coeluting reductase.

Characterization of the Apoprotein Adduct by ESI/ LC/MS Analysis. The P450 reaction mixtures were incubated with BPA or BMP in the absence (control) or presence (inactivated) of NADPH, and then analyzed by ESI/LC/MS.
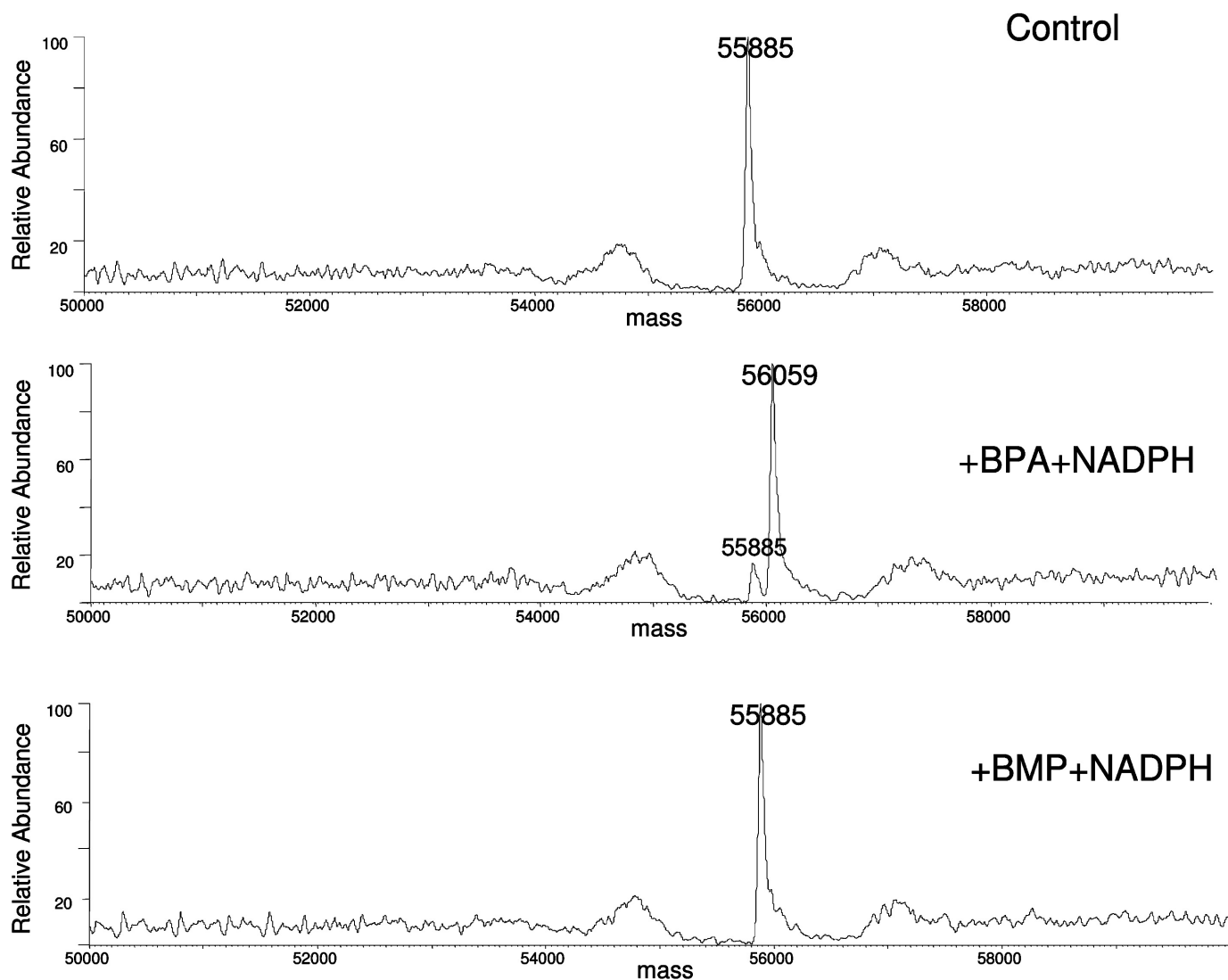
Fig. 6. ESI/LC/MS analysis of CYP2B1 apoprotein inactivated by BPA or BMP. The incubation conditions, HPLC, and MS analysis conditions were as described under *Materials and Methods*. A, representative deconvoluted mass spectrum from a control incubation of CYP2B1 with either BPA or BMP in the absence of NADPH. B, representative deconvoluted mass spectrum of P450 2B1 incubated with BPA in the presence of NADPH. C, representative deconvoluted mass spectrum of CYP2B1 incubated with BMP in the presence of NADPH.

Portions of the reaction mixtures were analyzed for EFC de-ethylation activity, and ~10% of the catalytic activity remained after the inactivation by either BPA or BMP. Figure 6A shows the unmodified CYP2B1 apoprotein with a mass of ~55,885 Da. Figure 6B shows the BPA-inactivated CYP2B1 apoprotein with the predominant mass of ~56,059 Da and a trace amount of unmodified protein with a mass of ~55,885 Da. The difference in the mass of ~174 Da is consistent with the addition of the mass of one BPA molecule plus one oxygen atom. In contrast, under the same conditions, Fig. 6C shows that the mass of BMP-inactivated CYP2B1 apoprotein remains at ~55,885 Da, which is identical to that of the unmodified apoprotein. For the T205A apoprotein, a mass increase of ~174 Da was also observed after the inactivation by BPA, but no changes were observed after inactivation by BMP (data not shown). Therefore, CYP2B1 WT and the T205A mutant are inactivated by BPA, but not by BMP, via adduction to apoprotein.

LC/MS/MS Analysis of GSH Conjugates of BPA and BMP. One approach used to identify reactive intermediates

formed during metabolism by P450s involves trapping the intermediates by reaction with GSH and then elucidating the structures of the GSH conjugates by LC/MS/MS. Our laboratory has previously used this approach to identify the GSH conjugates formed during the inactivation of various P450s by a variety of ethynyl inactivators (Kent et al., 2006; Lin and Hollenberg, 2007; Sridar et al., 2008). Therefore, the formation of GSH conjugates during the inactivation of WT and T205A CYP2B1 by BPA and BMP was investigated.

The extracted ion chromatogram of a GSH conjugate eluting at 25.8 min with a precursor ion at m/z 482 is shown in Fig. 7A. This conjugate was observed during the inactivation of the WT and T205A mutant by BPA. The molecular mass of the GSH conjugate corresponds to the sum of the mass of GSH (307 Da) plus BPA (158 Da) and one oxygen. The MS/MS spectrum shown in Fig. 7B exhibits a fragment ion at m/z 407 from the loss of Gly (75 Da); the fragment ion at m/z 353 is from loss of Glu (129 Da); and the further loss of water forms the ion at m/z 335 (Baillie and Davis, 1993). The ion at m/z 278 is from a combination of the loss of Glu and Gly, and

A Extracted ion chromatogram
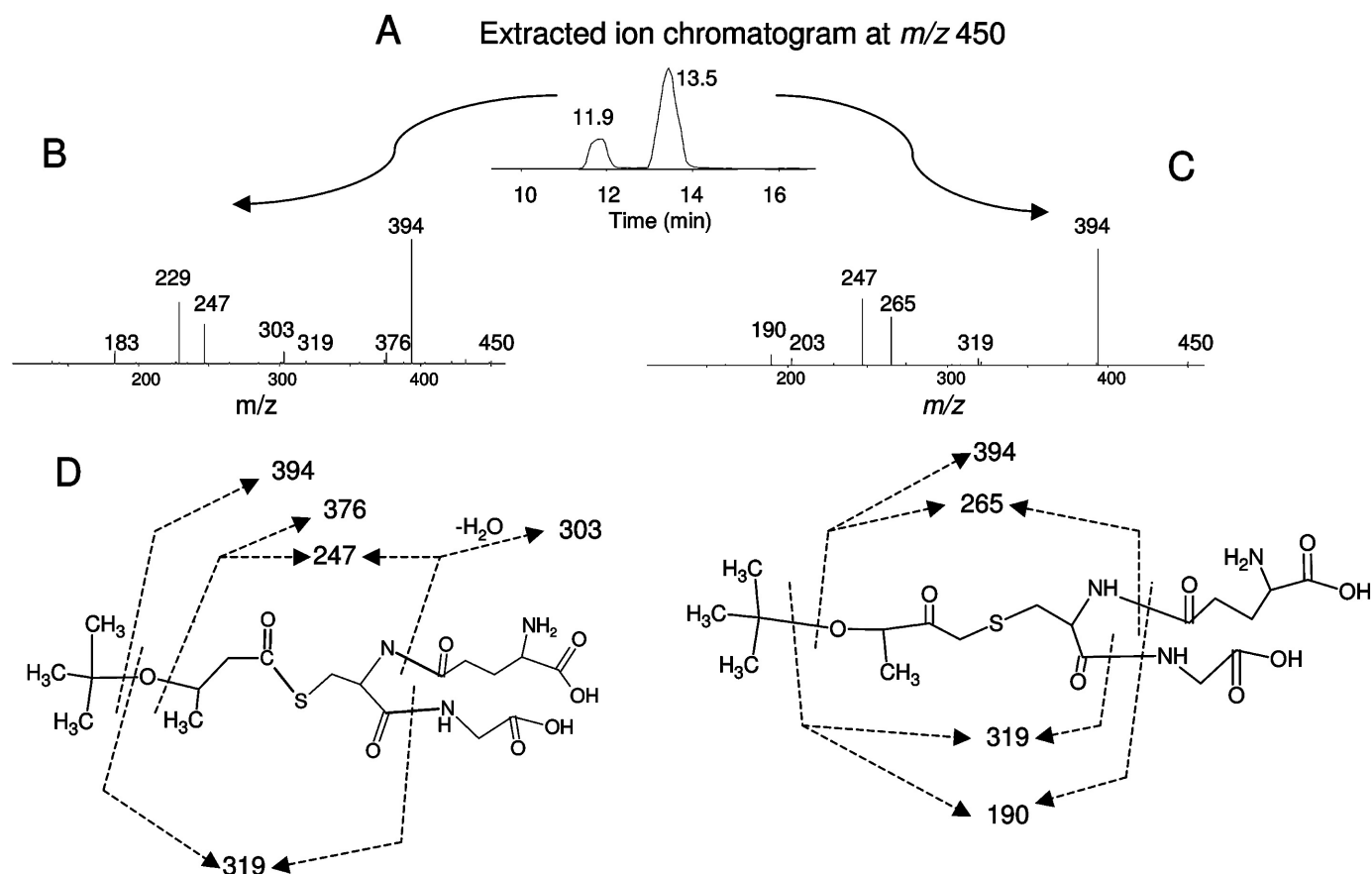
B MS/MS spectrum
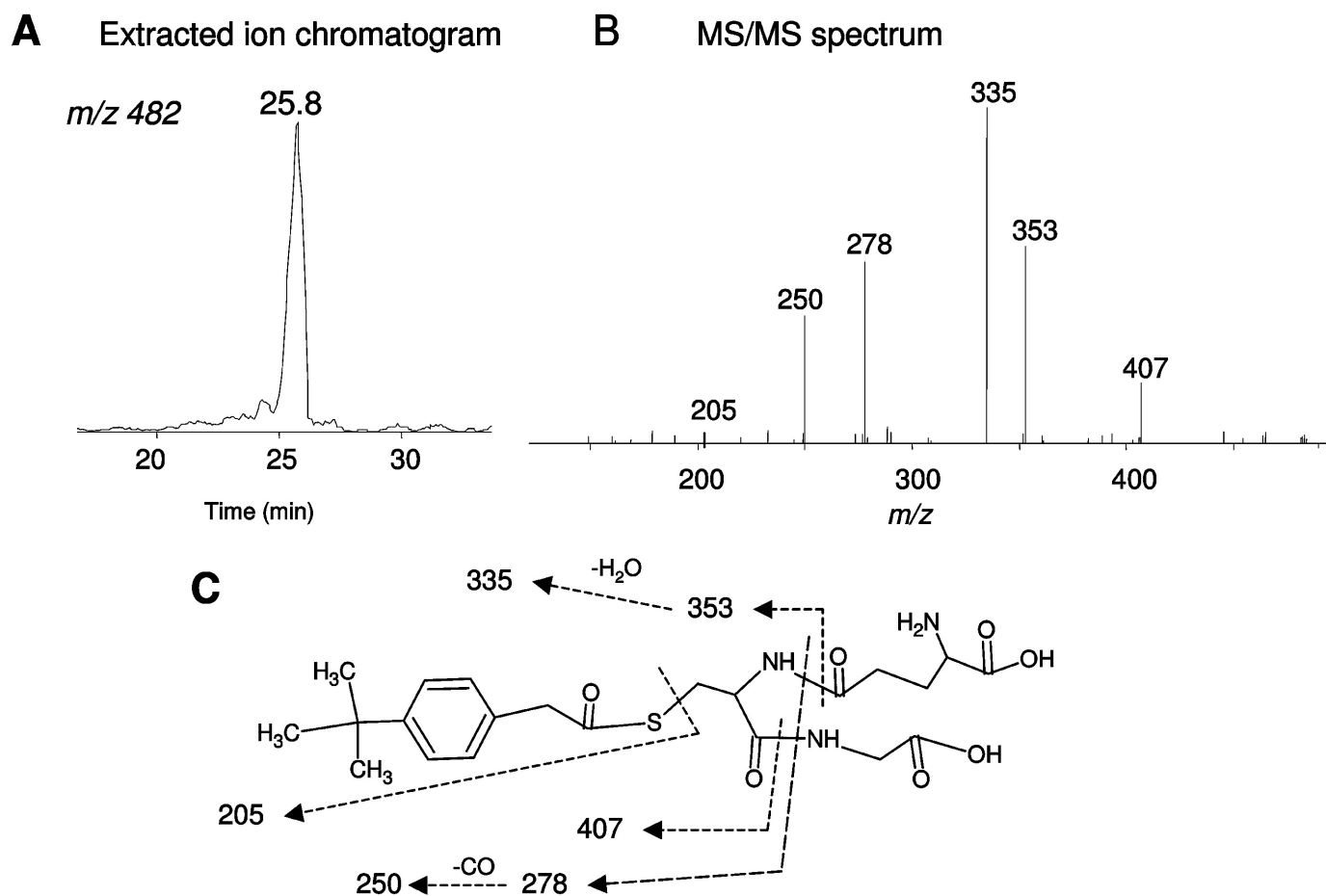
Fig. 7. LC/MS/MS analysis of a GSH conjugate of BPA formed by WT CYP2B1. A reaction mixture containing CYP2B1 was incubated with BPA in the presence of NADPH; the reactive intermediate was trapped with GSH; and the GSH conjugate was analyzed as described under *Materials and Methods*. A, extracted ion chromatogram of a GSH conjugate eluting at 25.8 min with the MH$^+$ ion at *m/z* 482. B, MS/MS spectrum of the GSH conjugate eluting at 25.8 min. C, proposed structure of the GSH conjugate. The dashed lines indicate the sites of fragmentation and are explained in the text. The MS/MS spectra were obtained in the positive mode and analyzed using the Xcalibur software package (Thermo Fisher Scientific).

the further loss of CO produces the fragment ion at *m/z* 250. All the fragment ions indicate that GSH is a component of the BPA-GSH conjugate at *m/z* 482. The ion at *m/z* 205 results from the cleavage of the C-S bond within the GSH moiety. However, whether the oxygen has been added to the internal or terminal carbon cannot be ascertained from the MS/MS spectrum. Ortiz de Montellano et al., (1982) have previously reported that if the oxygen atom is added to the internal carbon, the heme will be alkylated, and if the oxygen is added to the terminal carbon, the protein will be modified (Ortiz de Montellano and Komives, 1985; CaJacob et al., 1988; Chan et al., 1993). Because a protein adduct was identified in this case, the structure proposed for the GSH conjugate has the oxygen inserted into the terminal carbon as shown in Fig. 7C. The mass increase of 174 Da for the BPA-GSH conjugate is equivalent to the mass of BPA plus one oxygen and is identical to the mass increase of the apoprotein adduct in the inactivated P450, indicating that the same reactive species forming the GSH conjugate covalently binds with the P450 apoprotein.

The extracted ion chromatograms for the two GSH conjugates with precursor ions at *m/z* 450 formed in incubations of BMP with WT CYP2B1 are shown in Fig. 8A. Similar results were observed on incubations of BMP with the T205A mutant, except the relative intensity of the two conjugates was

almost identical (data not shown). The molecular mass of these two GSH conjugates corresponds to the sum of the mass of BMP plus one oxygen atom and GSH. The MS/MS spectra of the conjugates that eluted at 11.9 and 13.5 min are displayed in Fig. 8, B and C, respectively. For both GSH conjugates, the major fragment ion at *m/z* 394 is from the loss of a *tert*-butyl group, and the further loss of a Gly will give a fragment ion having *m/z* 319. The rest of the fragment ions are different between the conjugates, indicating that there are two GSH conjugate isomers. One GSH conjugate may be formed from the addition of the oxygen to the internal carbon, and the other derived from the addition of the oxygen to the terminal carbon of ethynyl moiety. The structures cannot be ascertained from the MS/MS spectrum. Two proposed structures for the GSH conjugates with the oxygen added to the internal or terminal carbon of ethynyl moiety are shown in Fig. 8D. The fragmentation sites leading to the formation of fragment ions at *m/z* 376, 303, 265, 247, and 190 are indicated by dashed lines. For the conjugate eluting at 11.9 min, the loss of water from the ion at *m/z* 247 will form an ion at *m/z* 229. For the conjugate eluting at 13.5 min, the loss of water from ion at *m/z* 265 will form an ion at *m/z* 247. Again, the presence of two distinct ions at *m/z* 183 (B) and *m/z* 203 (C) indicates a structural difference between these two conjugates. The ion at *m/z* 203 may be caused by the loss of Glu

Fig. 8. LC/MS/MS analysis of GSH conjugates of BMP formed by WT CYP2B1. A reaction mixture containing CYP2B1 was incubated with BMP in the presence of NADPH, and the reactive intermediates were trapped with GSH. The GSH conjugates were analyzed as described under *Materials and Methods*. A, extracted ion chromatogram of the GSH conjugates with the MH$^+$ ion at *m/z* 450 eluting at 11.9 and 13.5 min. B, MS/MS spectrum of the GSH conjugate eluting at 11.9 min. C, MS/MS spectrum of the GSH conjugate eluting at 13.5 min. D, proposed structure of the GSH conjugates. The dashed lines indicate the sites of fragmentation. The MS/MS spectra were obtained in the positive mode and analyzed using the Xcalibur software package (Thermo Fisher Scientific).

and water from a fragment ion of the CH$_2$CO moiety linked to the GSH at *m/z* 350 (Lin and Hollenberg, 2007). The ion at *m/z* 183 is probably part of the GSH moiety. The mass increase of 142 Da, equivalent to the mass of oxygenated BMP, for the GSH-BMP conjugate is identical to the mass increase seen for the heme adducts, indicating that the same reactive species forming the GSH-BMP conjugate can also *N*-alkylate the pyrrole rings in the heme. Although the reactive species with oxygen added to the terminal carbon of ethynyl moiety is detected, the lack of protein modification may be the result of the absence of nucleophilic residues in the active site or their distance from the site of formation of the reactive intermediate or their reactivity.

Discussion

The importance of the Thr205 residue in CYP2B1 has been previously shown in studies that show it plays a role in the 16β-hydroxylation activity of testosterone and androstenedione and in the mechanism-based inactivation of CYP2B1 by 17α-ethynylestradiol (Lin et al., 2003, 2004). Here, the mechanism-based inactivation of WT CYP2B1 by two structurally related *tert*-butyl acetylenic compounds, BPA and BMP, and the effect of the mutation of Thr205 to Ala on the inactivation were investigated. Both BPA and BMP are very effective mechanism-based inactivators of CYP2B1. However, the ef-

ficiency of the inactivation is ~100-fold greater and the partition ratio is 10-fold less with BPA than with BMP, indicating that BPA is a more potent mechanism-based inactivator than BMP. The inactivation of CYP2B1 by BPA is a result of covalent binding of BPA to the apoprotein, and the inactivation by BMP is caused by the formation of multiple heme adducts. It is of interest to note that BMP also inactivates CYP2E1 (Blobaum et al., 2002), whereas BPA does not (H. L. Lin and P. F. Hollenberg, unpublished observation).

The mutation of Thr205 to Ala leads to a decrease in k_{inact} of ~4-fold for both BMP and BPA. There is no significant change in the K_I of BMP, whereas there is a dramatic increase in the K_I of BPA. Thus, the mutation of Thr205 has a much more profound effect on the efficiency of inactivation (k_{inact}/K_I) by BPA than that by BMP. Although the T205A mutation did not change the formation of heme adduct peak 2, the formation of heme adduct peak 1 during inactivation by BMP was markedly suppressed, indicating that the regioselectivity for the *N*-alkylation of the pyrrole rings by the reactive oxygenated intermediate of BMP was altered by the Thr to Ala conversion.

To facilitate the interpretation of the experimental data, we constructed a CYP2B1 homology model based on the crystal structure of CYP2B4 (Scott et al., 2004). The structure of the distal surface of CYP2B1, showing the location of

A

BPA

B

BMP
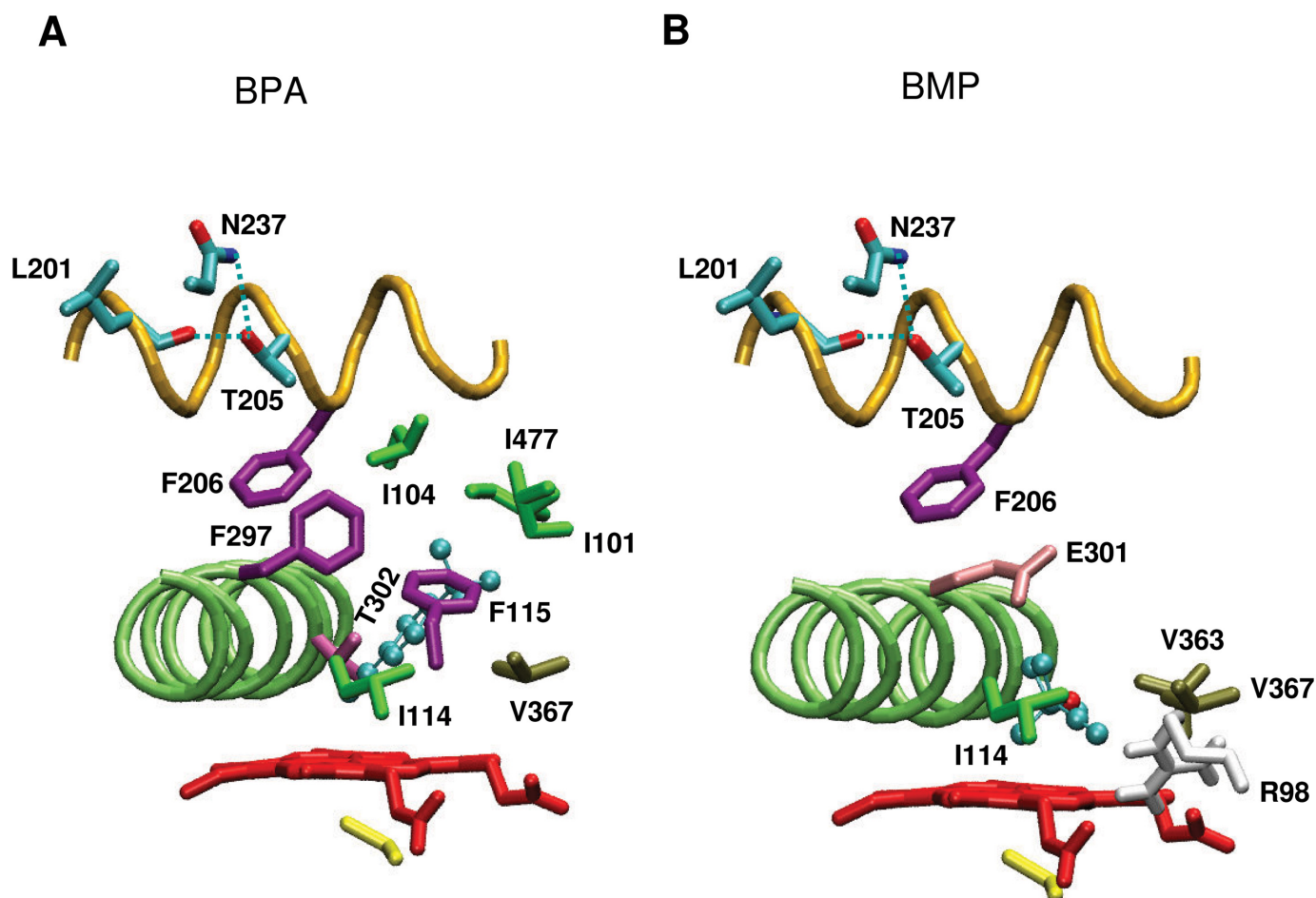
Fig. 9. Homology modeling and docking studies of BPA (A) and BMP (B) into the CYP2B1 active site. Leu201, Thr205, and Phe206 are F-helix residues. Phe297, Glu301, and Thr302 are I-helix residues. Two hydrogen bonds are indicated by blue dashed lines: 1) between Thr205 and Leu201; 2) between Thr205 and Asn237. Residues within 3.5 Å of BPA are Ile101, Ile104, Ile114, Phe115, Phe297, Thr302, Val367, and Ile477. Residues within 3.5 Å of BMP are Arg98, Ile114, Glu301, Val363, and Val367. Shown in color are BPA and BMP (cyano), F-helix (orange), I-helix (green), heme (red), and the axial Cys436 (yellow).

Leu201, Thr205, and Phe206 in the F-helix, the location of Asn237 in the G-helix, and the location of Phe297, Glu301, and Thr302 in the I-helix, is displayed in Fig. 9. Docking studies suggest that the triple bond of BPA is positioned within the active site at an angle of ~60° and a distance of 2.96 Å from the heme iron (Fig. 9A), whereas the triple bond in BMP displays a favored orientation that is almost parallel to the heme plane (Fig. 9B). The differences between the orientations of the triple bonds in the active site may explain why protein modification is favored during inactivation by BPA, whereas heme alkylation is favored during inactivation by BMP. Both BPA and BMP have *tert*-butyl side chains; however, the difference between BPA and BMP is the presence of the phenyl and methyl-ether moieties, respectively. It appears that this difference has a tremendous effect on the orientation of the substrates in the active site. Residues in the active site within 3.5 Å of BPA are Ile101, Ile104, Ile114, Phe115, Phe297, Thr302, V367, and Ile477. Residues in the active site within 3.5 Å of BMP are Arg98, Ile114, Glu301, Val363, and Val367. All these residues fall within the putative substrate recognition sites (SRS) proposed by Gotoh (1992). The possible reasons for the lower K_I with BPA than with BMP are as follows: 1) BPA is more hydrophobic than BMP such that it is probably more tightly bound in the active

site than BMP; 2) BPA bound in the active site is in close contact with more SRS residues than BMP; and 3) site-directed mutagenesis studies have shown that residues Ile101, Ile104, Phe115, Phe297, and Thr302, which are all within 3.5 Å of BPA, are very critical for CYP2B1 substrate entry, substrate specificity, and for determining metabolite profiles (Domanski et al., 2001; Johnson, 2003; Honma et al., 2005). Unlike BPA, which is a *tert*-butyl-substituted phenylacetylene, phenylacetylenes substituted with a methyl, chloro, or nitro groups *para-* to the ethynyl group all inactivate CYP2B1 in the reconstituted system by *N*-alkylation of the prosthetic heme group (Komives and Ortiz de Montellano, 1987). Therefore, differences in the mechanisms of inactivation of a single P450 can be substrate-specific and can be altered by relatively small differences in the structure of the inactivator.

Homology modeling studies show that Thr205 participates in hydrogen bonding to the two residues Leu201 and Asn237. Moreover, the Phe206, adjacent to Thr205, is a critical SRS-2 residue for CYP2B1 catalysis (He et al., 1995; Domanski and Halpert, 2001). Leu201 and Phe206 are located in the F-helix, and Asn237 is located in the G-helix. The conversion of Thr205 to an Ala not only disrupts the hydrogen bonding between the F- and G-helices but also may move the Phe206

away from the active site. As a consequence, the overall conformational change in these regions may alter both substrate access to the active site and the binding orientations of substrates within the active site. Thus, the k_{inact} values for the inactivation of the mutant by both BPA and BMP were decreased. After the Thr to Ala conversion, the K_I for inactivation by BPA increased ~25-fold, whereas there was no change for BMP. As shown in Fig. 9A, docking studies of BPA suggest that Phe206 is very close to Phe297 and that the three residues Phe297, Ile104, and Phe115 are close to each other. The change in the conformation of Phe206 on the replacement of Thr205 by Ala may affect the conformation of the Phe297, Ile104, and Phe115 residues and thereby alter the hydrophobic interactions between BPA and residues closest to it. However, Phe297, Ile104, and Phe115 are not in close contact with BMP (Fig. 9B). When Thr205 was substituted with Ala, the loss of stability of protein-substrate binding site caused by the interactions between residues Phe206, Phe297, Ile104, and Phe115 would be expected to have a higher impact on the binding affinity of BPA than of BMP. Therefore, it appears that the docking analyses are consistent with our experimental results.

Previous studies have shown that BMP inactivates CYP2B4 as a result of the formation of two heme adducts in which N-alkylation of pyrrole rings A and D is suggested to occur (Von Weymarn et al., 2004). Ortiz de Montellano et al. (1982) have shown the formation of three metal-free regioisomers as a result of prosthetic heme alkylation after administration of ethchlorvynol to phenobarbital-treated rats. The first two isomers, which eluted very close together by HPLC, are identified as structures with the N-alkyl group on the vinyl-substituted pyrrole rings (A and B). The third isomer is identified as a structure with the N-alkyl group either on the C or D ring. In this study, LC/MS/MS analysis has revealed the formation of three different Fe-free heme adducts, suggesting that oxygenated BMP also N-alkylates three of the four pyrrole rings. The HPLC elution profile of the heme adducts formed by the inactivation of CYP2B1 by BMP is very similar to that observed for the inactivation of hepatic microsomal P450 by ethchlorvynol. The results presented here suggest that BMP destroys the CYP2B1 heme by alkylating three of the pyrrole nitrogens. Our docking studies suggest that the C ring is much more favored to be alkylated than the D ring. Thus, we postulate that rings A, B, and C were alkylated. As shown in Fig. 4, the amount of heme adduct peak 2, corresponding to alkylation of the C ring, is about the same in both WT and T205A, whereas the formation of heme adduct peak 1, corresponding to alkylation of rings A and B, is 10-fold lower in the T205A mutant than in the WT, indicating that the Thr205 to Ala conversion selectively suppressed the N-alkylation of rings A and B. Perhaps, the disruption of Thr205-Leu201 and Thr205-Asn237 hydrogen bonding caused by the conversion of Thr205 to Ala may alter the conformation in the F-G region for BMP entering the substrate access channel. As a consequence, the orientation of the BMP triple bond may be steered away from rings A and B in the heme pocket. In short, Thr205 plays an important role in the regiochemistry of heme alkylation by BMP.

In conclusion, BPA and BMP inactivate CYP2B1 very effectively. BPA causes inactivation as a result of covalent binding of the activated BPA to the P450 apoprotein, whereas BMP causes inactivation as a result of N-alkylation of the pyrrole rings. The results presented here further show the importance of the F-helix residues in catalysis by CYP2B1. The inactivation of CYP2B1 by BPA was caused by the formation of an adducted protein that exhibits a mass increase of 174 Da, which is equivalent to the addition of BPA plus one oxygen atom. LC/MS/MS studies that identify Thr302 as the residue covalently modified by the reactive intermediate of BPA will be presented in a subsequent publication.

References

Baillie TA and Davis MR (1993) Mass spectrometry in the analysis of glutathione conjugates. *Biol Mass Spectrom* **22:**319–325.

Blobaum AL, Kent UM, Alworth WL, and Hollenberg PF (2002) Mechanism-based inactivation of cytochromes P450 2E1 and 2E1 T303A by *tert*-butyl acetylenes: characterization of reactive intermediate adducts to the heme and apoprotein. *Chem Res Toxicol* **15:**1561–1571.

CaJacob CA, Chan WK, Shephard E, and Ortiz de Montellano PR (1988) The catalytic site of rat hepatic lauric acid ω-hydroxylase: protein versus prosthetic heme alkylation in the ω-hydroxylation of acetylenic fatty acids. *J Biol Chem* **263:**18640–18649.

Chan WK, Sui Z, and Ortiz de Montellano PR (1993) Determinants of protein modification versus heme alkylation: inactivation of cytochrome P450 1A1 by 1-ethynylpyrene and phenylacetylene. *Chem Res Toxicol* **6:**38–45.

Domanski TL and Halpert JR (2001) Analysis of mammalian cytochrome P450 structure and function by site-directed mutagenesis. *Curr Drug Metab* **2:**117–137.

Domanski TL, He YQ, Scott EE, Wang Q, and Halpert JR (2001) The role of cytochrome 2B1 substrate recognition site residues 115, 294, 297, 298, and 362 in the oxidation of steroids and 7-alkoxycoumarins. *Arch Biochem Biophys* **394:**21–28.

Gotoh O (1992) Substrate recognition sites in cytochrome P450 family 2 (CYP2) proteins inferred from comparative analysis of amino acid and coding nucleotide sequences. *J Biol Chem* **267:**83–90.

Guengerich FP, Hanna IH, Martin MV, and Gillam EM (2003) Role of glutamic acid 216 in cytochrome P450 2D6 substrate binding and catalysis. *Biochemistry* **42:**1245–1253.

Haines DC, Tomchick DR, Machius M, and Peterson JA (2001) Pivotal role of water in the mechanism of P450BM-3. *Biochemistry* **40:**13456–13465.

He YQ, He YA, and Halpert JR (1995) Escherichia coli expression of site-directed mutants of cytochrome P450 2B1 from six substrate recognition sites: substrate specificity and inhibitor selectivity studies. *Chem Res Toxicol* **8:**574–579.

Honma W, Li W, Liu H, Scott EE, and Halpert JR (2005) Functional role of residues in the helix B′ region of cytochrome P450 2B1. *Arch Biochem Biophys* **435:**157–165.

Johnson EF (2003) The 2002 Bernard B. Brodie Award lecture. Deciphering substrate recognition by drug-metabolizing cytochrome P450. *Drug Metab Dispos* **31:**1532–1540.

Kent UM, Lin HL, Mills DE, Regal KA, and Hollenberg PF (2006) Identification of 17α-ethynylestradiol modified active site peptides and glutathione conjugates formed during metabolism and inactivation of P450 2B1 and 2B6. *Chem Res Toxicol* **19:**279–287.

Kent UM, Mills DE, Rajnarayanan RV, Alworth WL, and Hollenberg PF (2002) Effect of 17α-ethynylestradiol on activities of cytochrome P450 2B (P4502B) enzymes: characterization of inactivation of P450s 2B1 and 2B6 and identification of metabolites. *J Pharmacol Exp Ther* **300:**549–558.

Kirton SB, Kemp CA, Tomkinson NP, St-Gallay S, and Sutcliffe MJ (2002) Impact of incorporating the 2C5 crystal structure into comparative models of cytochrome P450 2D6. *Proteins* **49:**216–231.

Komives EA and Ortiz de Montellano PR (1987) Mechanism of oxidation of π bonds by cytochrome P450. Electronic requirements of the transition state in the turnover of phenylacetylenes. *J Biol Chem* **262:**9793–9802.

Lin HL and Hollenberg PF (2007) The inactivation of cytochrome P450 3A5 by 17α-ethynylestradiol is cytochrome b_5-dependent: metabolic activation of the ethynyl moiety leads to the formation of glutathione conjugates, a heme adduct, and covalent binding to the apoprotein. *J Pharmacol Exp Ther* **321:**276–287.

Lin HL, Kent UM, and Hollenberg PF (2002) Mechanism-based inactivation of cytochrome P450 3A4 by 17α-ethynylestradiol: evidence for heme destruction and covalent binding to protein. *J Pharmacol Exp Ther* **301:**160–167.

Lin HL, Kent UM, Zhang H, Waskell L, and Hollenberg PF (2004) The functional role of threonine-205 in the mechanism-based inactivation of P450 2B1 by two ethynyl substrates: the importance of the F helix in catalysis. *J Pharmacol Exp Ther* **311:**855–863.

Lin HL, Zhang H, Waskell L, and Hollenberg PF (2003) Threonine-205 in the F helix of P450 2B1 contributes to androgen 16β-hydroxylation activity and mechanism-based inactivation. *J Pharmacol Exp Ther* **306:**744–751.

Lindberg RL and Negishi M (1989) Alteration of mouse cytochrome P450coh substrate specificity by mutation of a single amino-acid residue. *Nature* **339:**632–634.

Morris GM, Goodsell DS, Huey R, and Olson AJ (1996) Distributed automated docking of flexible ligands to proteins: parallel application of AutoDock 2.4. *J Comput Aided Mol Des* **10:**293–304.

Ortiz de Montellano PR, Beilan HS, and Mathews JM (1982) Alkylation of the prosthetic heme in cytochrome P450 during oxidative metabolism of sedative-hypnotic ethchlorvynol. *J Med Chem* **25:**1174–1179.

Ortiz de Montellano PR and Komives EA (1985) Branchpoint for heme alkylation and metabolite formation in the oxidation of arylacetylenes by cytochrome P-450. *J Biol Chem* **260:**3330–3336.

Roberts ES, Alworth WL, and Hollenberg PF (1998) Mechanism-based inactivation of cytochromes P450 2E1 and 2B1 by 5-phenyl-1-pentyne. *Arch Biochem Biophys* **354:**295–302.

Scott EE, He YA, Wester MR, White MA, Chin CC, Halpert JR, Johnson EF, and Stout CD (2003) An open conformation of mammalian cytochrome P450 2B4 at 1.6-Å resolution. *Proc Natl Acad Sci U S A* **100:**13196–13201.

Scott EE, White MA, He YA, Johnson EF, Stout CD, and Halpert JR (2004) Structure of mammalian cytochrome 2B4 complexed with 4-(4-chlorophenyl)imidazole at 1.9-Å resolution: insight into the range of P450 conformations and the coordination of redox partner binding. *J Biol Chem* **279:**27294–27301.

Silverman RB (1996) Mechanism-based enzyme inactivation, in *Contemporary Enzyme Kinetics and Mechanisms* (Purich DL ed) pp 291–335, Academic Press, San Diego, CA.

Spatzenegger M, Liu H, Wang Q, Debarber A, Koop DR, and Halpert JR (2003) Analysis of differential substrate selectivities of CYP2B6 and CYP2E1 by site-directed mutagenesis and molecular modeling. *J Pharmacol Exp Ther* **304:**477–487.

Sridar C, Kent UM, Noon K, McCall A, Alworth B, Foroozesh M, and Hollenberg PF (2008) Differential inhibition of cytochromes P450 3A4 and 3A5 by the newly synthesized coumarin derivatives 7-coumarin propargyl ether and 7-(4-trifluoromethyl)coumarin propargyl ether. *Drug Metab Dispos* **36:**2234–2243.

von Weymarn LB, Blobaum AL, and Hollenberg PF (2004) The mechanism-based inactivation of P450 2B4 by *tert*-butyl 1-methyl-2-propynyl ether: structural determination of the adducts to the P450 heme. *Arch Biochem Biophys* **425:**95–105.

Von Weymarn LB, Sridar C, and Hollenberg PF (2004) Identification of amino acid residues involved in the inactivation of cytochrome P450 2B1 by two acetylenic compounds: the role of three residues in nonsubstrate recognition sites. *J Pharmacol Exp Ther* **311:**71–79.

Zhao Y and Halpert JR (2007) Structure-function analysis of cytochromes P450 2B. *Biochim Biophys Acta* **1770:**402–412.

Zhao Y, White MA, Muralidhara BK, Sun L, Halpert JR, and Stout CD (2006) Structure of microsomal cytochrome P450 2B4 complexed with the antifungal drug bifonazole: insight into P450 conformational plasticity and membrane interaction. *J Biol Chem* **281:**5973–5981.

Address correspondence to: Paul F. Hollenberg, Department of Pharmacology, 2301 MSRB III, 1150 West Medical Center Drive, Ann Arbor, MI 48109-5632. E-mail: phollen@umich.edu